Triangulenium dyes: the comprehensive photo-absorption and emission story of a versatile family of chromophores

Irina Barsuk, Philippe Lainé, François Maurel, Eric Brémond

Journal Name

ARTICLE TYPE

Cite this: DOI: 00.0000/xxxxxxxxxx

Triangulenium Dyes: the Comprehensive Photo-Absorption and Emission Story of a Versatile Family of Chromophores†

Irina Barsuk,[a] Philippe P. Lainé,[a] François Maurel[a] and Éric Brémond*[a]

Received Date
Accepted Date

DOI: 00.0000/xxxxxxxxxx

The triangulenium dyes constitute a family of versatile chromophores whose impressive photo-absorption and emission properties are currently highlighted in numerous novel experimental applications. In this investigation, we provide a comprehensive TDDFT characterization of their spectrocopic properties elucidating the origin of their large and complex absorption and emission vibronic spectra spread over the (whole) visible region. More precisely, by benchmarking the performance of 10 commonly-used exchange-correlation density functionals belonging to different classes of approximation, we develop and validate a computational protocol allowing the accurate modeling of both the position and optical line-shape of their vibrationally-resolved absorption and emission band structures. We find that semilocal approximations provide the best estimate of the structure of the vibronic spectra, however they spuriously and strongly underestimate their position. We finally show that global-hybrid density functionals mixing between 20 and 30% of exact-like exchange are an excellent compromise to get a satisfactory estimate of both of these properties.

1 Introduction

Triangulenium (TA) dyes belong to the very large triarylcarbenium family of organic cationic dyes.[1] Their name derives from their characteristic triangular and planar molecular structure which originates from an intramolecular *ortho*-condensation of a triarylcarbenium scaffold.[2–5] Despite the cationic character of their central carbon atom, triangulenium dyes are recognized to be highly stable compounds in solution.[6] Their (electronic) structure is indeed stabilized by a resonant and extended electronic conjugation delocalized over their whole planar platform. They become thus sensitive-less to nucleophilic attacks and proved to be 'exceptionally' stable in polar solvents.[7]

Owing to their originality and uncommon electronic features, triangulenium dyes have become key organic compounds of great scientific and industrial importance. The large efforts dedicated to their functionalization made indeed their versatile reputation,[5,8,9] and started their popularization in numerous fields of research in chemistry. The tuning of their side positions by substituting electron donor groups allows for example to improve their cytotoxicity as DNA intercalating agents,[10–12] their photocatalytic activity as photosynthesizers,[13–15] or their long fluorescence lifetimes as fluorophores.[16–18]

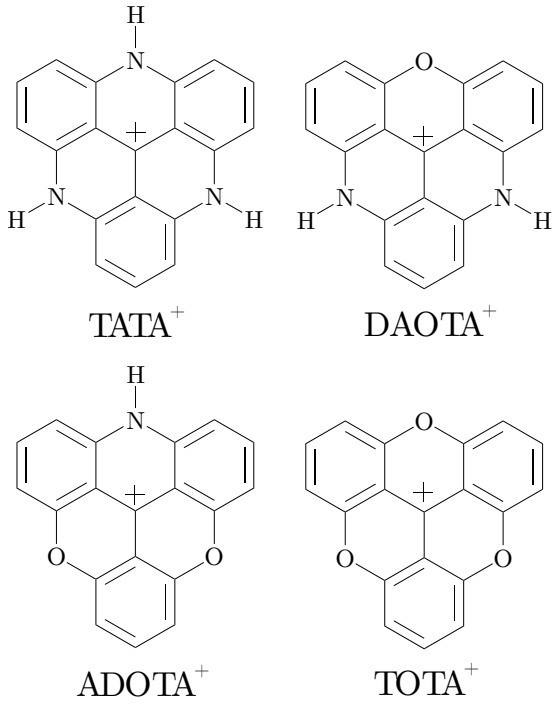

Fig. 1 Representation of the triangulenium carbocations investigated herein.

[a] *Université de Paris, ITODYS, CNRS, F-75006 Paris, France. E-mail: eric.bremond@u-paris.fr*

† Electronic Supplementary Information (ESI) available: [details of any supplementary information available should be included here]. See DOI: 00.0000/00000000.

Except from some still rare exceptions,[19,20] most of the triangulenium synthesis reported in literature focus on an oxo- and/or aza-bridging of the 3 aryl groups of a triarylcarbenium reactant.[2,3] The resulting bare 4,8,12-triaza- ($TATA^+$), 4,8-diaza-12-oxo- ($DAOTA^+$), 4-aza-8,12-dioxo- ($ADOTA^+$), and 4,8,12-trioxo ($TOTA^+$) trianguleniums are depicted in Fig. 1. All of them are distinguished by their own impressive spectroscopic features.[21–24] Their UV/vis signature is indeed experimentally characterized by a large, complex and intense absorption band spreading within the visible region.[23] An excess of nitrogen-based bridges (*e.g.*, $TATA^+$ and $DAOTA^+$) tends to red-shift the position of the absorption maximum while their replacement by oxygen atoms (*e.g.*, $TOTA^+$, $ADOTA^+$) shifts the band to the opposite blue direction. The origin of the complex absorption band shape depends however on many factors deriving both from the experimental conditions and the structure of the dye in solution. If the formation of ion pairs[25] or self-aggregates[26] are proved to be at the origin of some spectral features under certain experimental conditions, we are going to demonstrate in this investigation that the main contribution to the line shape of the UV/vis absorption spectrum comes from the vibrational and thermal effects.

Up to now, the main efforts dedicated to the modeling of the absorption and emission spectra of triangulenium dyes mainly focused on the computation of vertical excitations.[21] In reference to more sophisticated post-Hartree-Fock approaches, they find that the linear-response time-dependent (TD) variant[27,28] of density-functional theory[29,30] (DFT) provides a fair estimate of the first low-lying singlet-singlet transition occurring in N-methyl-substituted ADOTA and DAOTA derivatives. More precisely, they show that the local $\pi \rightarrow \pi^\star$ character of the first vertical excitation is well described by global-hybrid density functionals mixing between 20 and 30% of exact-like exchange (EXX), and thus confirm for this family of dyes, the methodological trends derived from years of benchmarking and tests dealing with dye chemistry.[31–33]

However, the vertical approximation in TDDFT provides here a crude estimate of the position of the experimental maximum of absorption.[21] It leads one to believe that the large energy error observed between theory and experiment comes from neglecting the vibrational and thermal effects. An improvement to the vertical approximation estimate consist indeed in computing the 0–0 energy which corresponds to the adiabatic energy difference between the lowest vibrational level of the excited and ground states. It is formally calculated by summing the difference of zero-point vibrational energy of each considered electronic state to the adiabatic energy. Numerous benchmark investigations showed that the 0–0 energy is a large theoretical improvement with respect to the vertical approximation when targeting the accurate modeling of the experimental maximum of absorption or emission of a vibrationally-resolved spectrum.[34–39] They thus confirm that global-hybrid density functionals mixing roughly $\sim$25% of EXX are the best approaches to accurately model an experimental reference.

Actually, the 0–0 energy is recognized as part of the "best energy estimate" of the maximum of a UV/vis absorption spectrum but this quantity does not provide any information regarding the line shape of a vibrationally-resolved absorption or emission spectrum. The convolution of the 0–0 transition by a Gaussian function is a first approximation to the problem.[40] The model conserves the advantage to be computationally inexpensive. However, it is unable to reproduce the vibronic fine structure of a band. Within the TDDFT framework, it is common practice to approximate a vibrationally-resolved spectrum by computing the resulting Franck-Condon factors, *i.e.*, the overlap integrals between ground- and excited-vibrational eigenvectors, and broadening them with a temperature-dependent Gaussian distribution function.[41–43] Over the last decade, the approach has been extensively developed and popularized by Barone, Bloino and Biczysko.[44–47] Pushed by methodological investigations[48–51] and the concomitant implementation of the analytical TDDFT Hessian matrix,[52] it allowed to comprehensively understand the UV/vis absorption and emission signatures of several large organic and organometallic chromophores,[53–55] and to go beyond with the accurate simulation of intuitive parameters such as the perceived colors of dyes in solution.[56–58]

In this investigation, we want to take advantage of the state-of-the-art quantum chemistry toolbox to establish a robust computational protocol allowing a comprehensive understanding of the large and complex vibrationally-resolved photo-absorption and emission spectra of triangulenium dyes. More precisely, we want to show our interest in the rationalization of the UV/vis spectroscopic properties of the most popular core compounds of the triangulenium dyes, *i.e.* the bare $TATA^+$, $DAOTA^+$, $ADOTA^+$ and $TOTA^+$ carbocations (Fig. 1), with the aim to provide a clear guideline for future investigations dealing with this versatile and very promising family of dyes.

2 Computational Details

Table 1 List of the exchange-correlation density functionals benchmarked in this investigation.

Name	Year	Type[§]	% EXX	Ref.
SVWN5	1980	LDA	0	59,60
PBE	1996	GGA	0	61
B3LYP	1993	GH-GGA	20	62–64
PBE0	1999	GH-GGA	25	65,66
M06	2008	GH-mGGA	27	67
BMK	2004	GH-mGGA	42	68
M06-2X	2008	GH-mGGA	54	67
M06-HF	2006	GH-mGGA	100	69,70
CAM-B3LYP	2004	RSH-GGA	19–65	71
ωB97XD	2008	RSH-GGA+D	22–100	72

[§] List of acronyms: LDA: local density approximation, GGA: generalized gradient approximation, mGGA: meta-GGA, +D: addition of an empirical dispersion correction, GH: global hybrid, RSH: range-separated hybrid.

All the computations are performed with the release B.01 of the Gaussian'16 program[73] using a tight self-consistent field (SCF) convergence criteria and an ultrafine integration grid. To establish our computational protocol we selected a broad panel composed by 10 widespread (semi)local, global- and range-separated hybrid density functionals reported in Table 1. Except when mentioned, the selected density functionals were associated with the 6-31+G* double-ζ basis set[74–77] which is generally recognized as an excellent trade-off between accuracy and computational

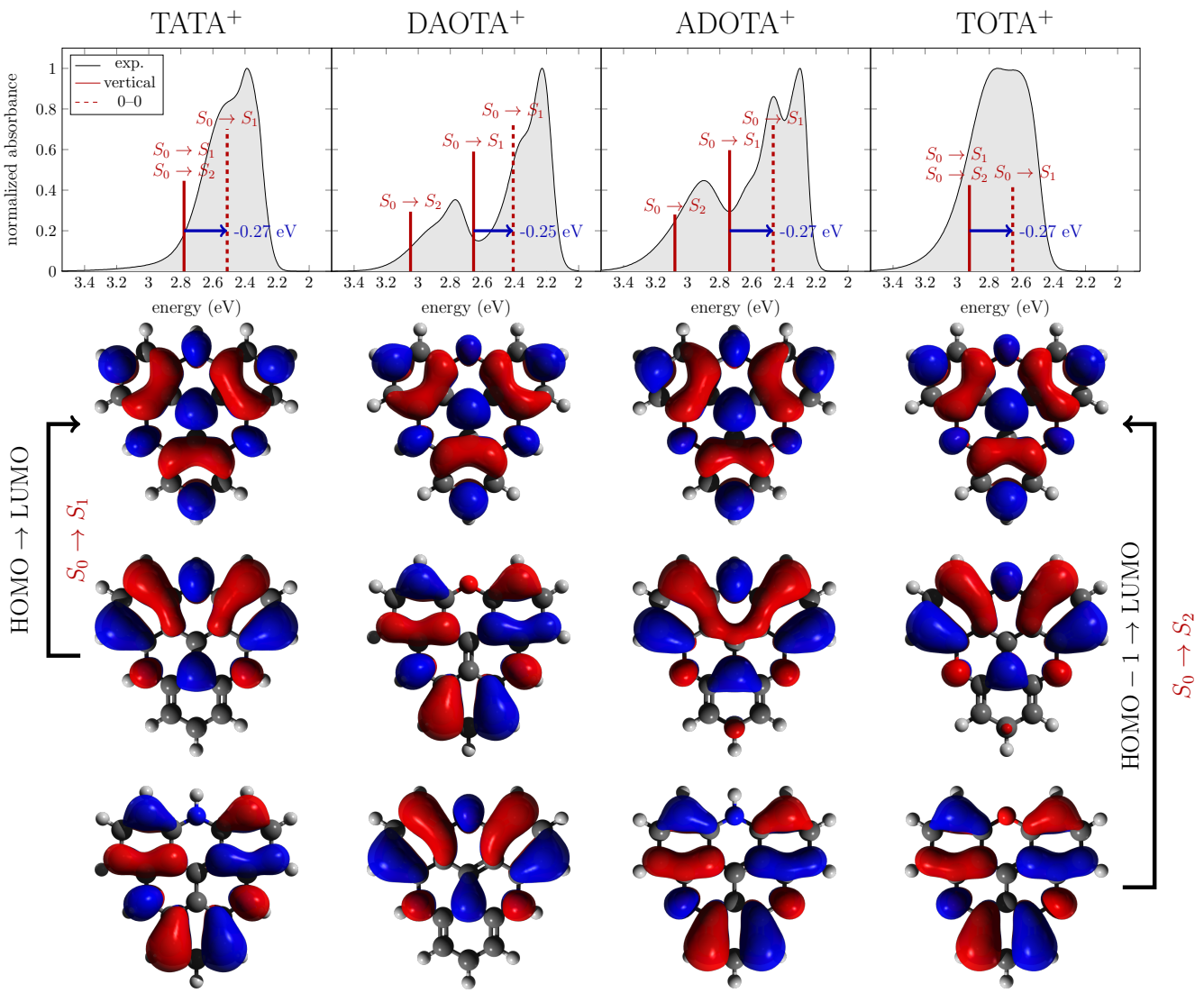

Fig. 2 Experimental absorption spectra of the TATA$^+$, DAOTA$^+$, ADOTA$^+$ and TOTA$^+$ triangulenium carbocations,[23] and the corresponding vertical $S_0 \rightarrow S_n$ and 0–0 $S_0 \rightarrow S_1$ transitions computed at the PCM-PBE0/6-31+G* level of theory in acetonitrile solvent. At the bottom of each spectra are represented the corresponding (top) LUMO, (middle) HOMO, and (bottom) HOMO-1 computed at the PCM-PBE0/6-31+G* level of theory in acetonitrile solvent. Molecular orbitals are plotted using an isosurface value set to 0.02 a.u.

efforts,[31] and as adequate in the specific case of the triangulenium dyes since a double-ζ basis set is proved to provide converged TDDFT vertical excitations.[21] Solvent effects were added by means of the polarizable continuum model (PCM) using the integral equation formalism (IEF),[78,79] setting up, except in specific cases, the dielectric constant as the one of the acetonitrile solvent.

Following the D_{3h} (C_{2v}) symmetry point group, the ground-state structures of the TATA$^+$ and TOTA$^+$ (DAOTA$^+$ and ADOTA$^+$) triangulenium carbocations are first fully optimized at DFT. Their optimized geometries are then confirmed as energy minimum structures by computing the corresponding Hessian matrix and verifying the absence of imaginary vibrational modes. Similarly, the first-singlet-excited-state structures of the triangulenium dyes considered herein are fully optimized and characterized at TDDFT level restricting their point group symmetry to C_s. The vibrationally-resolved one-photon absorption and emission spectra are obtained within the Franck-Condon (FC) and Franck-Condon–Herzberg-Teller (FCHT) approximation using the adiabatic Hessian model as implemented in the Gaussian'16 software.[41] More precisely, the vibronic computations are performed following a sum-over-states approach[42,80,81] in which each vibronic transition is classified into a "class" governing the number of simultaneously excited modes in the final state. The convergence of the band-shaped spectra is assured by setting the prescreening criteria of transition selection to 25 and 20 quanta for the first and second classes, respectively, and fixing the maximum number of integrals to 1×10^8. During the density-functional benchmark investigation, the envelope of each spectrum is evaluated at room temperature (298.15 K) with a Gaussian distribution

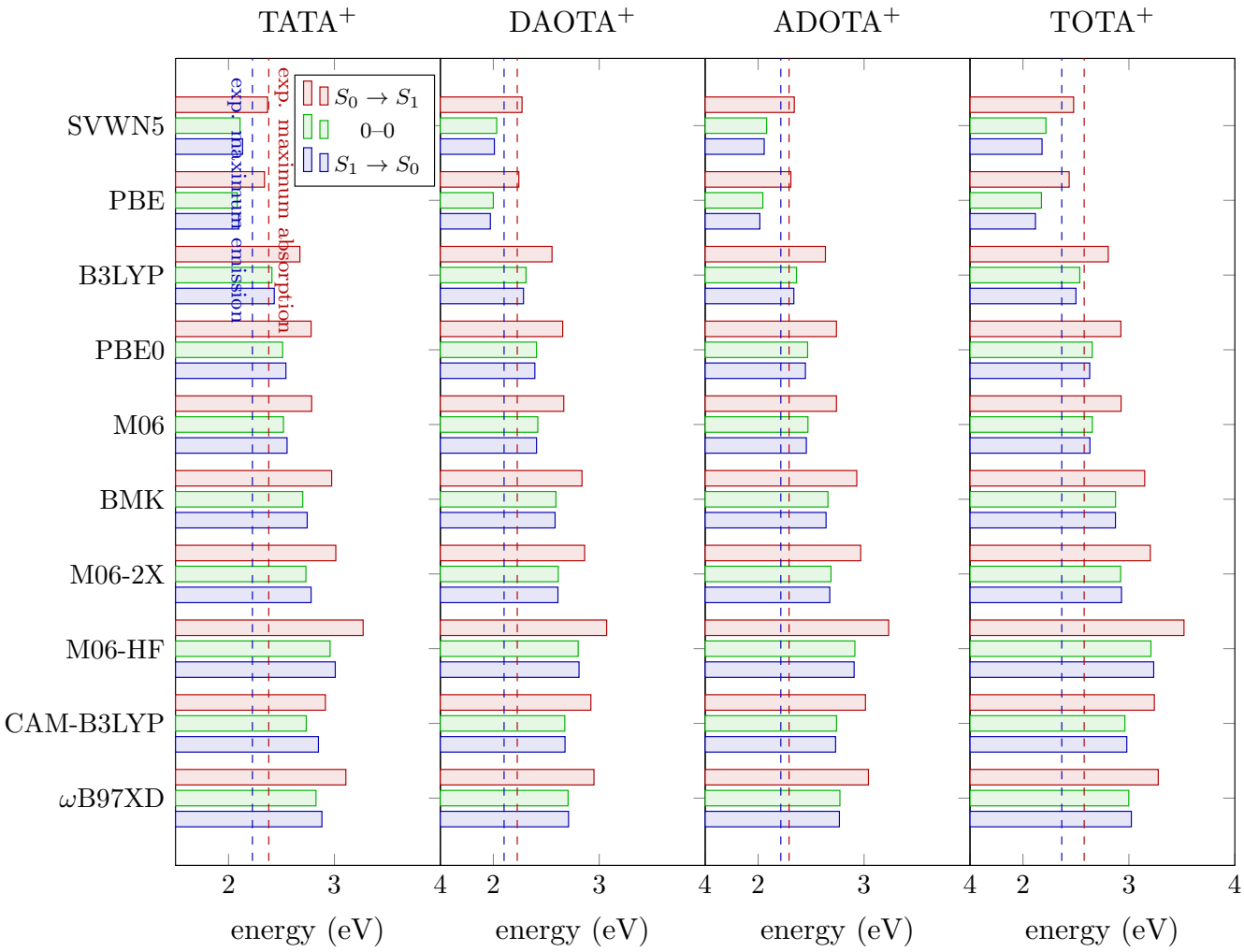

Fig. 3 (red) Vertical $S_0 \rightarrow S_1$ absorption, (green) first 0–0 vibronic transition, and (blue) vertical $S_1 \rightarrow S_0$ emission energies (eV) computed for the selected density functionals with the 6-31+G* basis set in PCM acetonitrile solvent, within the TDDFT framework. Experimental (red dashed line) absorption and (blue dashed line) emission energies of the first low-lying bands are reported as reference and taken from Ref. 23.

function whose full width of half maximum (FWHM) is set to 250 cm^{-1}. However the latter parameter is set to 500 cm^{-1} when the comparison is done with the experimental references derived from Ref. 23 in order to reproduce the experimental broadening.

3 Results and Discussion

Within the visible domain, the experimental absorption spectra of the 4 triangulenium carbocations (Fig. 1) investigated herein appear like a broad and intense vibrationally well-resolved absorption band lying between 3.4 and 2.0 eV, *i.e.*, 365 and 620 nm, respectively (Fig. 2). To get a first qualitative idea of the TDDFT performance with respect to this family of chromophores, we start by computing their TDDFT vertical absorption spectra in acetonitrile solvent from their ground-state-optimized structures with the PBE0 global hybrid, a density functional recommended as an excellent compromise by numerous benchmark investigations both for its accuracy in modeling ground- and excited-state structures,[82,83] and vertical excitations of large organic dyes.[31–33] Depending on the compound, the large experimental absorption band is modeled by one or two singlet–singlet vertical excitations. In agreement with their D_{3h} ground-state symmetry structures, the computed absorption spectra of $TATA^+$ and $TOTA^+$ correspond to a degenerate $S_0 \rightarrow S_1$ vertical excitation governed by a $\pi \rightarrow \pi^\star$ transition of HOMO $\rightarrow$ LUMO and HOMO $-1 \rightarrow$ LUMO types (Fig. 2). They lie around 2.78 eV for the former and 2.92 eV for the latter while the experimental reference are measured at 2.38 and 2.58 eV, respectively. The N-alkylation of $TATA^+$ by a methyl or *n*-propyl group to better reproduce the experimental conditions reported in Ref. 23 (*i.e.*, N-propylated $TATA^+$) does not improve at all the estimation of the position of the maximum of absorption. In both cases, the first vertical excitation is computed at 2.76 eV, showing thus the negligible impact (0.02 eV) of the N-alkylation on the absorption spectrum. All in all, PBE0 provides a poor estimate of the experimental reference and largely overestimates it by more than 0.3 eV.

The reduction of the point group symmetry going from D_{3h} (*e.g.*, $TATA^+$ and $TOTA^+$) to C_{2v} (*e.g.*, $DAOTA^+$ and $ADOTA^+$)

Table 2 Mean signed deviation (MSD in eV), mean absolute deviation (MAD in eV), and maximum deviation (MAX in eV) energies calculated over the 4 triangulenium dyes considered herein with the selected 10 density functionals using the 6-31+G* basis set in PCM acetonitrile solvent. The vertical and 0–0 absorption approximations take as a reference the experimental maximum of absorption while the vertical series uses the experimental maximum of emission as a reference. 23. The roman number code in parenthesis refers to (I): TATA$^+$, (II): DAOTA$^+$, (III): ADOTA$^+$, and (IV): TOTA$^+$.

	SVWN5	PBE	B3LYP	PBE0	M06	BMK	M06-2X	M06-HF	CAM-B3LYP	ωB97XD
vertical absorption approximation ($S_0 \rightarrow S_1$)										
MSD	-0.00	-0.04	0.30	0.41	0.41	0.60	0.64	0.90	0.65	0.73
MAD	0.05	0.05	0.30	0.41	0.41	0.60	0.64	0.90	0.65	0.73
MAX	-0.10 (IV)	-0.14 (IV)	0.34 (III)	0.45 (III)	0.45 (III)	0.64 (III)	0.68 (III)	0.94 (IV)	0.72 (III)	0.75 (III)
0–0 absorption approximation ($S_0 \rightarrow S_1$)										
MSD	-0.26	-0.29	0.04	0.14	0.15	0.34	0.37	0.60	0.41	0.46
MAD	0.26	0.29	0.06	0.14	0.15	0.34	0.37	0.60	0.41	0.46
MAX	-0.36 (IV)	-0.40 (IV)	0.08 (II)	0.18 (II)	0.19 (II)	0.37 (III)	0.40 (III)	0.63 (IV)	0.45 (II)	0.48 (III)
vertical emission approximation ($S_1 \rightarrow S_0$)										
MSD	-0.27	-0.32	0.02	0.13	0.14	0.34	0.38	0.62	0.44	0.48
MAD	0.27	0.32	0.06	0.13	0.14	0.34	0.38	0.62	0.44	0.48
MAX	-0.40 (IV)	-0.46 (IV)	-0.08 (IV)	0.17 (II)	0.18 (II)	0.36 (I)	0.40 (I)	0.66 (IV)	0.47 (I)	0.50 (I)

drastically modify the main features of the experimental absorption spectra (Fig. 2). The former large and intense experimental band is here splitted in two, a first intense at low energy and a second whose intensity is merely divided by a factor 3 at larger energy. The PBE0 global-hybrid density functional reproduces these main spectral features and models both of them by two well distinct and largely spaced (∼0.4 eV) $S_0 \rightarrow S_1$ and $S_0 \rightarrow S_2$ vertical excitations whose oscillator strengths reproduce the intensity decrease in going from the first to the second band. As observed for TATA$^+$ and TOTA$^+$, both vertical excitations are of $\pi \rightarrow \pi^\star$ type and are ruled by a HOMO $\rightarrow$ LUMO and HOMO $-1 \rightarrow$ LUMO transition, respectively. The $S_0 \rightarrow S_1$ energies are computed at 2.66 and 2.74 eV for DAOTA$^+$ and ADOTA$^+$, respectively, while the experimental maxima of absorption are measured at 2.23 and 2.29 eV, respectively, showing here again a large overestimation of the reference by more than 0.4 eV. The alkylation of the nitrogen centers does not provide any improvement, the vertical transition being here insensitive to this parameter. The same trend is also observed for the $S_0 \rightarrow S_2$ energies. Indeed, they are computed at 3.05 and 3.08 eV for DAOTA$^+$ and ADOTA$^+$, respectively, while the maxima of the second experimental bands are acquired at 2.77 and 2.90, respectively.

In all cases, the large energy deviations obtained between theory and experiment originate from the crude approximation provided by the vertical excitation model. The very large absorption bands observed experimentally are indeed prone to important vibrational effects which can be taken into account through the computation of the 0–0 energy, that is the difference in energy between the lowest vibrational level of each considered singlet state. Computing this quantity with PBE0 corresponds to a red-shift of the $S_0 \rightarrow S_1$ vertical energy of about 0.25 eV for DAOTA$^+$ and 0.27 eV for the 3 other triangulenium dyes (Fig. 2). The estimation of the maximum of absorption of the first absorption band becomes thus 2.51, 2.41, 2.47 and 2.65 eV for TATA$^+$, DAOTA$^+$, ADOTA$^+$ and TOTA$^+$, respectively. With respect to the experimental reference, PBE0 still overestimates the position of the maximum of absorption of the first absorption band, however the deviations are merely decreased to ∼0.1 eV, recovering thus the range of errors promised by the TDDFT benchmarks regarding the optical 0–0 transitions in solvated dyes.[35]

Beyond the qualitative point of view, we assess here the performance of 10 commonly used density functionals in estimating the photo-absorption and emission energy properties of the 4 triangulenium dyes through the computation of the vertical absorption, 0–0, and vertical emission energy properties. We not only base this density-functional selection thanks to their popularity, but also because they constitute a broad and representative panel of the density-functional landscape depicted by the first four rungs of the Perdew's Ladder[84] of exchange-correlation approximations (Table 1). More precisely, we select 2 pure, 6 global-hybrid mixing between 20 and 100% of EXX, and 2 range-separated exchange hybrid approximations including one adding on-top an empirical dispersion correction. Figure 3 reports their performance to model excited-state energy properties and compares them with the related experimental references, *i.e.* the maximum of absorption and emission energies. Table 2 provides the corresponding statistical analysis of the density functional performance.

Within the vertical absorption approach, the local SVWN5 and semilocal PBE density functional approximations are found as the best to estimate the position of the maximum of absorption of the 4 triangulenium dyes. Both of them position the 4 maxima with an error not larger than 0.14 eV. These accurate estimates are however caused by an error compensation between the many-electron self-interaction error (SIE),[85] which strongly contaminates (semi)local approximations and provides a spurious lowering of the excited-state energy properties,[86] and the neglect of the vibrational effects. The other density functionals which belong to the global- and range-separated exchange hybrid approximations, strongly overestimates the position of the maxima of absorption, the best performer being B3LYP with an error not larger than 0.34 eV. As a general trend, we notice that the more a hybrid mixes a large fraction of EXX, the more it blue-shifts the energy of the vertical transition. B3LYP being the considered global hybrid mixing the lowest fraction of EXX (20%), it provides here the best estimate of the absorption maximum within the vertical approximation with a mean absolute deviation (MAD) of about 0.30 eV (Table 2). PBE0 (EXX = 25%) and M06 (EXX = 27%) just follow with a MAD equals to 0.45 eV. Density functionals mixing larger fractions of EXX get very poor performance with absolute

deviations larger than 0.5 eV.

The addition of the vibrational contributions through the computation of the 0–0 vibronic transition strongly improves the quality of the model. It demonstrates that (semi)local density functionals strongly underestimate the position of the experimental maximum of absorption due to the SIE.[86] In case of PBE (Table 2), the mean signed and maximum deviations (MSD and MAX, respectively) reach indeed -0.29 and -0.40 eV, respectively. As generally observed for gound-state properties,[87] the hybridization of the density functional largely improves the computed 0–0 vibronic energy. Indeed, B3LYP closely followed by PBE0 and M06 are found as the most accurate global hybrids with a MAD lower than 0.1 eV for the former and lower than 0.2 eV for the latter. Their best (worst) estimate of the position of the experimental maximum of absorption is found for the $TOTA^+$ ($DAOTA^+$) carbocation (Fig. 3). The performance of the global hybrids mixing larger fractions of EXX and range-separated hybrids remain disappointing with MAD larger than 0.4 eV.

With respect to the first (red edge) absorption band of the triangulenium dyes, the emission one experimentally measures is as much narrow,[23] letting thus think to a smaller importance of the vibrational contributions. This hypothesis is confirmed for all chromophores by the computation of the vertical de-excitation energy ($S_1 \rightarrow S_0$) from the optimized first-singlet-state C_s structure, the latter being structurally characterized by an asymmetric elongation of the heteroatom bridges. The vertical TDDFT emission energies computed with B3LYP, PBE0 and M06 are indeed found as the best to estimate the experimental maxima of emission with MADs ranging between 0.06 and 0.15 eV, the best density functional remaining B3LYP (Table 2). The performance trend with respect to the fraction of EXX is here again observed (Figure 3). It depicts a strong underestimation of the position of the maximum of emission for semi(local) approximations (EXX = 0%), an accurate estimation with global-hybrid approximations mixing between 20 and 27% of EXX, and a strong overestimation for global- and range-separated hybrid approximations mixing larger fraction of EXX.

In light of the TDDFT computational protocol raised to accurately position the UV/vis absorption and emission maxima of the 4 triangulenium carbocations, we propose now to go further in this electronic structure investigation by attempting the modeling of the band-shape of the spectra. From a methodological point of view, the latter property can be obtained through the computation of the Franck-Condon factors just followed by their temperature-dependent convolution with an inhomogeneous sum of Gaussian functions. The resulting spectral broadening adds thus to the vibrational effects, the temperature ones. The Franck-Condon factors are approximated following a Taylor expansion of the transition dipole moment around the equilibrium geometry of each electronic state, leading thus to the so-called Franck-Condon approximation (FC, order 0), or the Franck-Condon–Herzberg-Teller one (FCHT, order 1). Fig. 4 depicts the line shape of the first low-lying vibrationally-resolved absorption band of $TATA^+$ computed with the PBE0 density functional within the FC and FCHT approximations. In comparison with the experimental UV/vis absorption spectrum (Figure 2), it shows that the FCHT approach improves

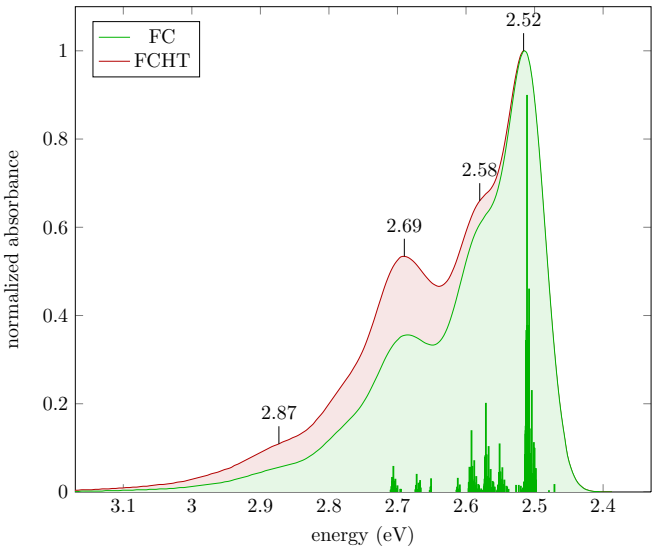

Fig. 4 Low-lying vibronic absorption band ($S_0 \rightarrow S_1$) of $TATA^+$ computed according to the (green) Franck-Condon (FC), and (red) Franck-Condon–Herzberg-Teller (FCHT) approaches at the PCM-TD-PBE0/6-31+G* level of theory in acetonitrile solvent at 298.15 K. The green stick spectrum corresponds to the vibronic transitions computed within the FC approach. The broadening of each spectrum is performed by a Gaussian convolution of each stick spectrum with FWHM = 250 cm^{-1}.

the FC one by increasing the relative intensities of the main shoulders of the absorption band positioned at 2.58, 2.69 and 2.87 eV, with a special emphasis on the one at 2.69 eV. It indicates that in this energy region, vibrational modes involving larger amplitude displacements exist and are important. Moreover, the comparison between the position of the maximum of absorption energy (2.52 eV) and the 0–0 one (2.51 eV) demonstrates that the thermal effects included through the inhomogeneous convolution are here very low (0.01 eV).

Up to now, the solvent effects were included through the PCM implicit solvation model setting by default the dielectric constant as the one of the acetonitrile solvent. Fig. 5 investigates the solvatochromic character of $TATA^+$ in order to understand how the polarity of the solvent influences its UV/vis absorption signature. Thanks to their cationic character, the spectroscopic properties of the triangulenium dyes in solution are experimentally studied in polar solvents like acetonitrile, DMSO or water.[3] In this way, their UV/vis signatures were shown to be insensitive to solvent effects. For dielectric constants larger than $\varepsilon = 35$ a.u., TDDFT at PBE0 level confirms this trend, and demonstrates that the position of the maximum of absorption is unchanged (*i.e.*, an energy deviation lower than 0.01 eV) with respect to the solvent. Only the relative intensity of the second shoulder (2.69 eV) of the low-lying band slightly decreases with the polarity of the solvent. Going to less polar solvents blue-shifts however the maximum of absorption by less than 0.04 eV and further increases the relative intensity of the second shoulder. We thus notice and confirm that the absorption properties of the triangulenium dyes are quasi-insensitive to the solvent nature (virtually no solvatochromism).

Another important parameter known to influence the position

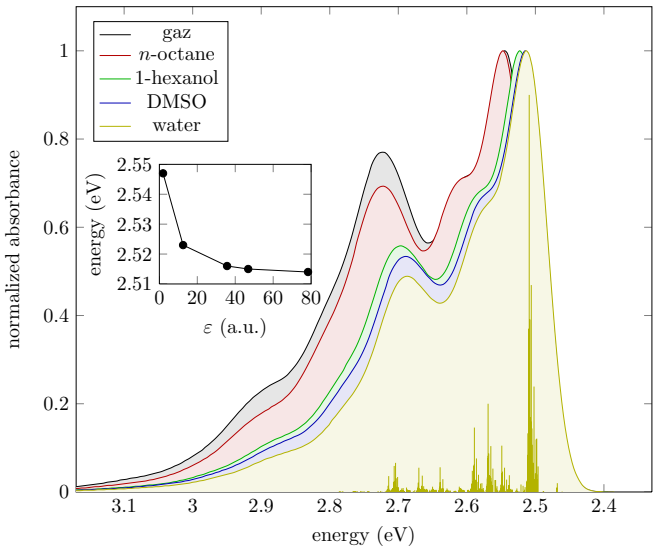

Fig. 5 Low-lying vibronic absorption band ($S_0 \rightarrow S_1$) of TATA$^+$ computed according to the Franck-Condon–Herzberg-Teller (FCHT) approach at the PCM-TD-PBE0/6-31+G* level of theory in (black) gas phase, or with a selection of solvents at 298.15 K. The orange stick spectrum corresponds to the vibronic transitions computed in PCM water solvent. The broadening of each spectrum is performed by a Gaussian convolution of each stick spectrum with FWHM $= 250$ cm^{-1}. The inset plots the maximum absorption energy (eV) function of the dielectric constant ε (a.u.) of the solvent.

and shape of the absorption band is the density-functional approximation. In the past, benchmark investigations performed on anthraquinone[50] and coumarine[48] families of dyes already showed that both properties cannot be both accurately modeled by the same approximation, and recommended the combination of PBE0 and ωB97XD to faithfully reproduce the 0–0 energy and optical line shape, respectively, of the absorption spectrum. Fig. 6 compares to experiments the performance of a subset composed by 5 density functionals to reproduce the UV/vis signature of the first low-lying absorption band of the 4 triangulenium carbocations within the FCHT approximation. The vibrationally-resolved absorption spectra obtained with the 5 other density functionals are reported in the electronic supplementary information (ESI).†

Since the position of the low-lying absorption band is directly related to the estimate of the 0–0 energy, it is first worth to notice that global-hybrid density functionals mixing between 20 and 30% of EXX such as B3LYP or PBE0 provide the best positioning of the band (Fig. 6). More precisely, a direct visual comparison with experiments shows that B3LYP is the most accurate to position the first vibrationally-resolved absorption band of TATA$^+$, DAOTA$^+$ and ADOTA$^+$ while PBE0 is found as the best to model this property in case of TOTA$^+$. For all chromophores, semilocal density-functional approximations such as PBE strongly red-shift the position of the band while global- and range-separated hybrids mixing larger fractions of EXX, *e.g.* M06-2X and ωB97XD, largely blue-shift it.

The comparison of the line shape of the band is visually more difficult to rationalize. Fixing a low value for the FWHM Gaussian parameter, *e.g.* FWHM $= 250$ cm^{-1}, allows however to track the main features of the absorption band. At first glance, the comparison of the line shape can be done through the determination of the relative position and intensity of the main shoulder with respect to the maximum of absorption (Fig. 6). All considered density functionals provide uniform results with respect to the position of the main shoulder. At ± 0.01 eV, they locate it at 0.17, 0.17, 0.18 and 0.14 eV from the position of the absorption maximum for TATA$^+$, DAOTA$^+$, ADOTA$^+$ and TOTA$^+$, respectively. The relative intensity differs however between each approximation. The more a density mixes a large fraction of EXX, the more the intensity of the main shoulder with respect to the maximum of absorption is low.

With respect to experiment, no density functional succeeds to faithfully model the line shape of the first low-lying absorption band of the triangulenium dyes with a broadening parameter set to FWHM $= 250$ cm^{-1} (Fig. 6). Only semilocal approximations (*e.g.*, PBE) could be *a priori* recommended as the best ones if the choice is based on the relative position and intensity of the main shoulder criteria. The agreement between theory and experiment could be however improved by varying the FWHM parameter. Increasing its value is indeed susceptible to improve the broadening in the region between the maximum of absorption and the main shoulder, and in consequence, to increase the intensity of the main shoulder. As a result, the modulation of this parameter is also susceptible to make global-hybrid density functionals mixing small fractions of EXX (*e.g.*, B3LYP and PBE0) suitable to get a matching picture of the band. Global- and range-separated hybrids mixing larger fractions of EXX (EXX $> 30\%$) are thus not recommended.

Indeed, doubling the value of the FWHM parameter, *i.e.*, FWHM $= 500$ cm^{-1}, improves the line shape agreement with experiments. Fig. 7 depicts it at the PBE0 level of theory for the first low-lying absorption and emission bands of the 4 carbenium chromophores. The shape of the vibrationally-resolved absorption band of TATA$^+$ and DAOTA$^+$ is in average in excellent agreement with experiments while it is less satisfactory reproduced for ADOTA$^+$ and TOTA$^+$. For the latter carbocations, we suspect that the observed deviations are caused by the harmonic approximation involved in the computation of the Franck-Condon factors. Their heteroatom bridges are indeed mainly made by C–O bonds whose potential deviates more from a harmonic behavior than the C–N ones.

A careful analysis of the main vibrational coupling modes at the origin of the complex shape of the absorption band provides more insights with respect to this hypothesis (Fig. 7). Out of the first coupling mode (*i.e.*, 16^1 for TATA$^+$ and 15^1 for the 3 other dyes) which corresponds to a symmetric planar breathing of the molecular skeleton, and contributes to the formation of the first small shoulder of the band (see Fig. 4 as an example), the two other main coupling modes involve, in increasing energy order, a planar asymmetric stretching and a symmetric bending of the C–X–C bridges, and are at the origin of the main shoulder of the absorption band. This analysis confirms thus that a lack of anharmonic treatments of the C–O–C bridges could be at the origin of the intensity depletion of the main shoulder of the absorption band in the case of ADOTA$^+$ and TOTA$^+$.

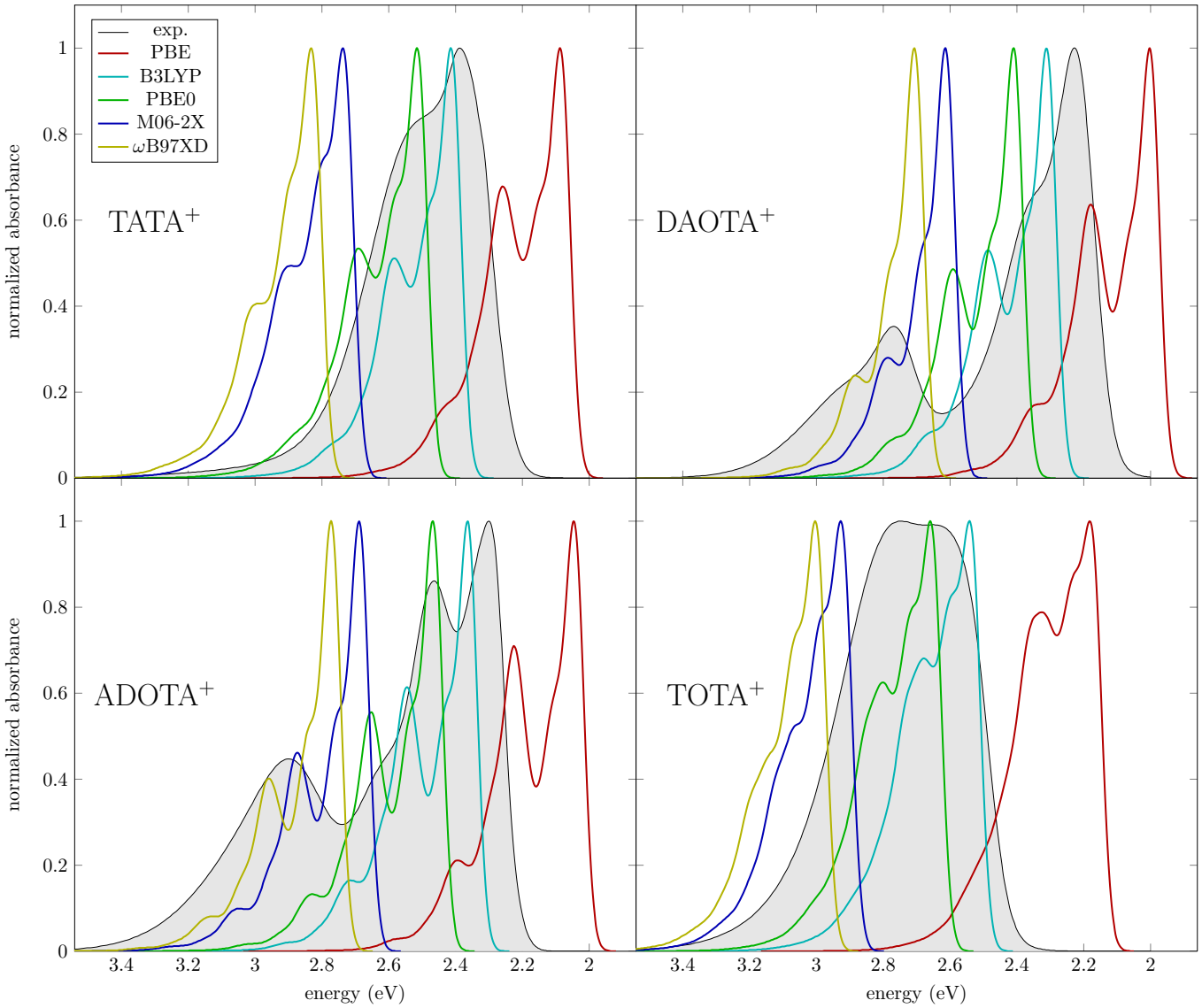

Fig. 6 Low-lying vibronic absorption bands ($S_0 \rightarrow S_1$) of the TATA$^+$, DAOTA$^+$, ADOTA$^+$ and TOTA$^+$ triangulenium carbocations computed with the Franck-Condon–Herzberg-Teller (FCHT) approach at 298.15 K with a selection of density functionals in combination with the 6-31+G* basis set and the PCM acetonitrile solvent, within the TDDFT framework. The broadening of each spectrum is performed by a Gaussian convolution with FWHM = 250 cm^{-1}. As a matter of comparison, the experimental absorption spectrum of each dye (in black) taken from Ref. 23 are reported.

The analysis of the emission band shape agrees with the previous conclusions (Fig. 7), even if the broadening is in overall less correctly reproduced. The relative intensity of the main shoulder is indeed strongly underestimated and affects here the 4 chromophores. As a result, the modeled emission band appears much more narrow than that observed experimentally, *i.e.*, its intensity vanishes around 2.2 eV while it vanishes at 1.8 eV at experimental level. It is worth noting that the intensity decrease of the main shoulder of each emission band impacts the evaluation of the Stokes shift. For the 4 triangulenium dyes, it is approximatively underestimated by ∼0.1 eV.

4 Conclusions

The triangulenium dyes constitute a family of versatile chromophores whose impressive photo-absorption and emission properties are currently highlighted in numerous novel experimental applications. Owing to their resonant and extended electronic conjugation delocalized over their whole planar platform, these carbocations not only exhibit a large, complex and intense absorption band lying in the visible region, but are also prone to very long fluorescence lifetimes. In this investigation, we provide for the first time a comprehensive theoretical characterization of their photo-absorption and emission properties, and develop and validate a computational protocol allowing the accurate modeling of their absorption and emission spectra at TDDFT level.

More precisely, we focus our efforts on the 4 bare triangulenium dyes used as starting building blocks in most of the photochemical investigations and commonly dubbed as TATA$^+$, DAOTA$^+$, ADOTA$^+$ and TOTA$^+$. As a first photochemical insight, we show that within the visible region, the complex shape of their

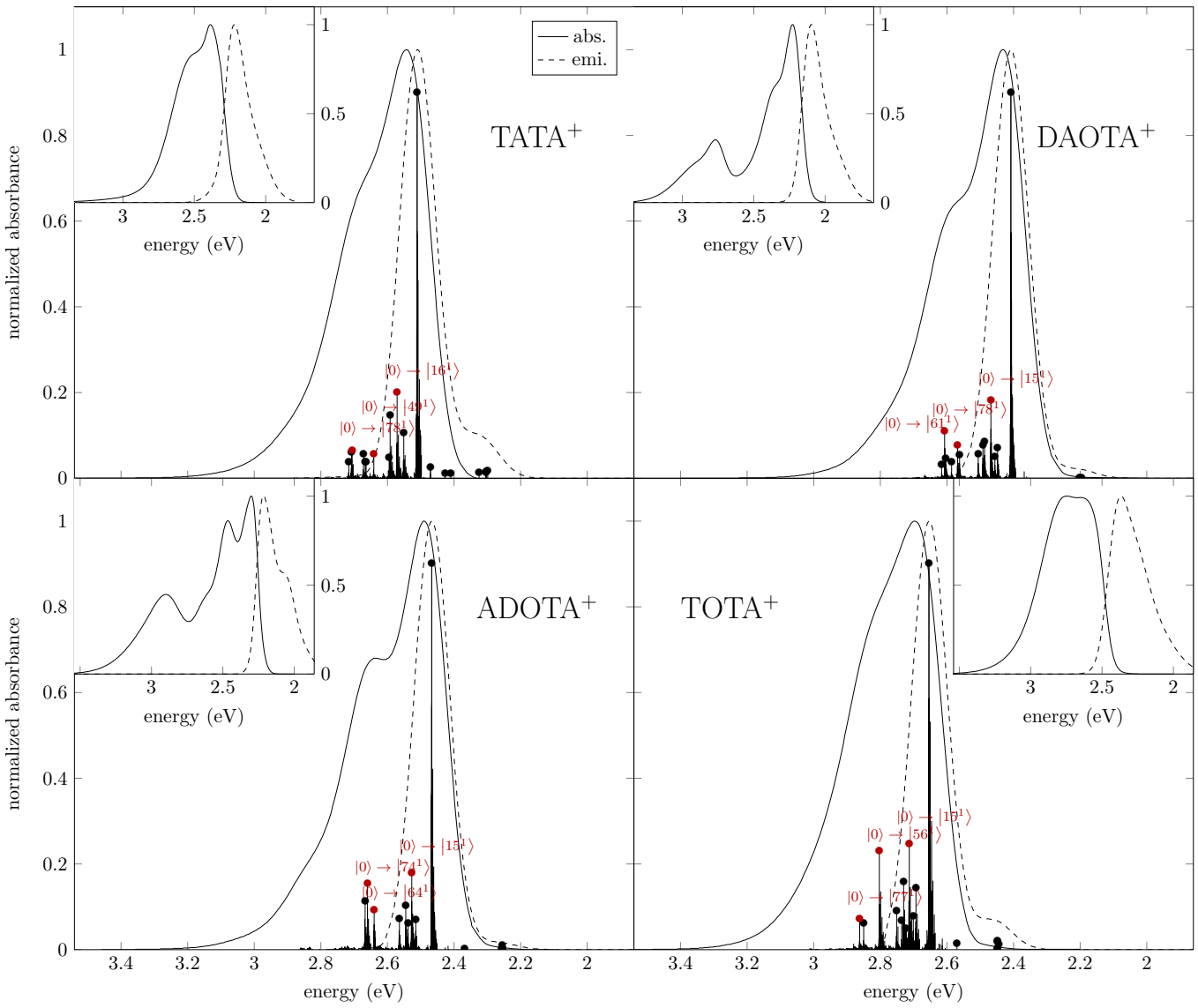

Fig. 7 Low-lying vibronic (solid line) absorption and (dashed line) emission bands of the TATA$^+$, DAOTA$^+$, ADOTA$^+$ and TOTA$^+$ triangulenium carbocations computed at 298.15 K with the Franck-Condon–Herzberg-Teller (FCHT) approach at the PCM-TD-PBE0/6-31+G* level of theory in acetonitrile solvent. The stick spectra corresponds to the computed vibronic transitions. Black and red dots are the main contributions to the stick spectrum with the corresponding numbers of the vibrational modes involved. The broadening of each spectrum is performed by a Gaussian convolution of each s tick spectrum with FWHM $= 500$ cm^{-1}. The insets depict the experimental absorption and emission spectra taken from Ref. 23.

absorption spectrum comes from the symmetry of their ground-state structure. Indeed, the UV/vis signature of TATA$^+$ and TOTA$^+$ (D_{3h}) originates from the first and degenerated singlet–singlet $\pi \rightarrow \pi^\star$ excitation, while reducing the symmetry of the compound to C_{2v} (DAOTA$^+$ and ADOTA$^+$), breaks the degeneracy and leads to a second blue-shifted and less intense absorption band. Moreover, by using the PCM implicit solvation model, we confirm that the triangulenium dyes are insensitive to the nature of the solvent (no solvatochromism) and go further by providing insights concerning the origin of their complex vibrationally-resolved absorption and emission band shapes. Within the Franck-Condon approach, the analysis of the main vibrational coupling modes demonstrates that the successive shoulders of the first absorption band of each chromophore results from the vibrational planar breathing of the platform, the planar asymmetric stretching and symmetric bending of the heteroatom bridges.

From a methodological point of view, we test here the performance of 10 commonly used exchange-correlation density functionals to model the photo-absorption and emission properties of the triangulenium dyes. We show that within the vertical approximation, TDDFT is unable to accurately position the absorption and emission bands of each dye. Indeed, the vibrational contributions reach here almost 0.3 eV and strongly impact the spectra. The computation of the 0–0 energy which corresponds to the vibronic transition between the lowest vibrational level of each singlet state provides here a better estimate of the position of the band. According to this approach, we demonstrate that global-

hybrid density-functional approximations casting between 20 and 30% of EXX, *e.g.*, B3LYP, PBE0 and M06, are the best compromise. In average, they provide an absolute error on the position of the maximum of absorption lower than 0.15 eV, the best one being B3LYP with MAD of about 0.06 eV. Similar performances are found with respect to emission properties.

In addition to the position of the first absorption and emission bands, we investigate also the modeling of their vibrationally-resolved features through the computation of the Franck-Condon factors still at TDDFT level. We demonstrate that the 0th order Franck-Condon approximation is not sufficient to accurately describe the complex shape of the band, and we recommend the Franck-Condon–Herzberg-Teller approach. Contrarily to previous published benchmark investigations,[48,50] we find that the lower the fraction of EXX mixed by a density-functional approximation is, the better the band-shape agreement with experiments is, the semilocal PBE approximation being the best to faithfully reproduced the absorption band shape. However, for the sake of methodological consistency, we recommend global hybrid approximations mixing between 20 and 30% of EXX like B3LYP, PBE0 or M06 as an excellent compromise in order to accurately estimate the position and optical line shape of the absorption signature of this dyes.

Among the 10 tested density functionals, we find that none of them are able to reproduce the large experimental width of the emission band. However, we show that global hybrid approximations mixing between 20 and 30% are again a good compromise to position it with an error lower 0.14 eV.

Conflicts of interest

There are no conflicts to declare.

Acknowledgements

The authors thank ANR (Agence Nationale de la Recherche) and CGI (Commissariat à l'Investissement d'Avenir) for their financial support of this work through Labex SEAM (Science and Engineering for Advanced Materials and devices) ANR-10-LABX-096, ANR-18-IDEX-0001. They acknowledge the GENCI-CINES for HPC resources (Projects A0040810359 and A0060810359).

Notes and references

1 D. F. Duxbury, *Chem. Rev.*, 1993, **93**, 381–433.
2 M. Stepien, E. Gonka, M. Zyta and N. Sprutta, *Chem. Rev.*, 2017, **117**, 3479–3716.
3 J. Bosson, J. Gouin and J. Lacour, *Chem. Soc. Rev.*, 2014, **43**, 2824–2840.
4 B. W. Laursen and T. J. Sørensen, *J. Org. Chem.*, 2009, **74**, 3183–3185.
5 B. Laursen and F. Krebs, *Angew. Chem. Int. Ed.*, 2000, **39**, 3432–3434.
6 J. C. Martin and R. G. Smith, *J. Am. Chem. Soc.*, 1964, **86**, 2252–2256.
7 B. W. Laursen, F. C. Krebs, M. F. Nielsen, K. Bechgaard, J. B. Christensen and N. Harrit, *J. Am. Chem. Soc.*, 1998, **120**, 12255–12263.
8 M. Rosenberg, M. Santella, S. A. Bogh, A. V. Muñoz, H. O. B. Andersen, O. Hammerich, I. Bora, K. Lincke and B. W. Laursen, *J. Org. Chem.*, 2019, **84**, 2556–2567.
9 R. Vanel, F.-A. Miannay, E. Vauthey and J. Lacour, *Chem. Commun.*, 2014, **50**, 12169–12172.
10 E. Leung, L. I. Pilkington, M. M. Naiya, D. Barker, A. Zafar, C. Eurtivong and J. Reynisson, *Med. Chem. Commun.*, 2019, **10**, 1881–1891.
11 A. Shivalingam, A. Vysniauskas, T. Albrecht, A. J. P. White, M. K. Kuimova and R. Vilar, *Chem. Eur. J.*, 2016, **22**, 4129–4139.
12 J. Reynisson, G. B. Schuster, S. B. Howerton, L. D. Williams, R. N. Barnett, C. L. Cleveland, U. Landman, N. Harrit and J. B. Chaires, *J. Am. Chem. Soc.*, 2003, **125**, 2072–2083.
13 C. Shao, Q. Xia, C. Qin and Z. Yang, *J. Phys. Chem. C*, 2020, **124**, 4050–4056.
14 R. Gueret, L. Poulard, M. Oshinowo, J. Chauvin, M. Dahmane, G. Dupeyre, P. P. Lainé, J. Fortage and M.-N. Collomb, *ACS Catalysis*, 2018, **8**, 3792–3802.
15 C. Adam, A. Wallabregue, H. Li, J. Gouin, R. Vanel, S. Grass, J. Bosson, L. Bouffier, J. Lacour and N. Sojic, *Chem. Eur. J.*, 2015, **21**, 19243–19249.
16 H. Noguchi, T. Hirose, S. Yokoyama and K. Matsuda, *CrystEngComm*, 2016, **18**, 7377–7383.
17 M. D. Hall, A. Yasgar, T. Peryea, J. C. Braisted, A. Jadhav, A. Simeonov and N. P. Coussens, *Methods Appl. Fluores.*, 2016, **4**, 022001.
18 R. M. Rich, D. L. Stankowska, B. P. Maliwal, T. J. Sørensen, B. W. Laursen, R. R. Krishnamoorthy, Z. Gryczynski, J. Borejdo, I. Gryczynski and R. Fudala, *Anal. Bioanal. Chem.*, 2013, **405**, 1618–2650.
19 M. Santella, E. Della Pia, J. K. Sørensen and B. W. Laursen, *Beilstein J. Org. Chem.*, 2019, **15**, 2133.
20 C. Nicolas, G. Bernardinelli and J. Lacour, *J. Phys. Org. Chem.*, 2010, **23**, 1049–1056.
21 S. A. Bogh, M. Simmermacher, M. Westberg, M. Bregnhøj, M. Rosenberg, L. De Vico, M. Veiga, B. W. Laursen, P. R. Ogilby, S. P. A. Sauer and T. J. Sørensen, *ACS Omega*, 2017, **2**, 193–203.
22 S. A. Bogh, I. Bora, M. Rosenberg, E. Thyrhaug, B. W. Laursen and T. J. Sørensen, *Methods Appl. Fluores.*, 2015, **3**, 045001.
23 E. Thyrhaug, T. J. Sørensen, I. Gryczynski, Z. Gryczynski and B. W. Laursen, *.J. Phys. Chem. A*, 2013, **117**, 2160–2168.
24 J. Reynisson, R. Wilbrandt, V. Brinck, B. W. Laursen, K. Nørgaard, N. Harrit and A. M. Brouwer, *Photochem. Photobiol. Sci.*, 2002, **1**, 763–773.
25 F. Westerlund, J. Elm, J. Lykkebo, N. Carlsson, E. Thyrhaug, B. Akerman, T. J. Sørensen, K. V. Mikkelsen and B. W. Laursen, *Photochem. Photobiol. Sci.*, 2011, **10**, 1963–1973.
26 J. B. Simonsen, F. Westerlund, D. W. Breiby, N. Harrit and B. W. Laursen, *Langmuir*, 2011, **27**, 792–799.
27 M. E. Casida, *Recent Advances in Density Functional Methods*, Chong, D. P., Ed., World Scientific: Singapore, 1995, vol. 1, pp. 155–192.

28 E. Runge and E. K. U. Gross, *Phys. Rev. Lett.*, 1984, **52**, 997–1000.

29 W. Kohn and L. J. Sham, *Phys. Rev. A*, 1965, **140**, 1133–1138.

30 P. Hohenberg and W. Kohn, *Phys. Rev. B*, 1964, **136**, 864–871.

31 C. Adamo and D. Jacquemin, *Chem. Soc. Rev.*, 2013, **42**, 845–856.

32 A. D. Laurent and D. Jacquemin, *Int. J. Quant. Chem.*, 2013, **113**, 2019–2039.

33 D. Jacquemin, E. A. Perpète, I. Ciofini and C. Adamo, *Acc. Chem. Res.*, 2009, **42**, 326–334.

34 D. Jacquemin, I. Duchemin and X. Blase, *J. Chem. Theory Comput.*, 2015, **11**, 5340–5359.

35 D. Jacquemin, A. Planchat, C. Adamo and B. Mennucci, *J. Chem. Theory Comput.*, 2012, **8**, 2359–2372.

36 R. Send, M. Kühn and F. Furche, *J. Chem. Theory Comput.*, 2011, **7**, 2376–2386.

37 L. Goerigk and S. Grimme, *J. Chem. Phys.*, 2010, **132**, 184103.

38 L. Goerigk, J. Moellmann and S. Grimme, *Phys. Chem. Chem. Phys.*, 2009, **11**, 4611–4620.

39 F. Furche and R. Ahlrichs, *J. Chem. Phys.*, 2002, **117**, 7433–7447.

40 É. Brémond, J. Kieffer and C. Adamo, *J. Mol. Struct. THEOCHEM*, 2010, **954**, 52 – 56.

41 A. Baiardi, J. Bloino and V. Barone, *J. Chem. Theory Comput.*, 2013, **9**, 4097–4115.

42 F. Santoro, R. Improta, A. Lami, J. Bloino and V. Barone, *J. Chem. Phys.*, 2007, **126**, 084509.

43 M. Dierksen and S. Grimme, *J. Phys. Chem. A*, 2004, **108**, 10225–10237.

44 C. Puzzarini, J. Bloino, N. Tasinato and V. Barone, *Chem. Rev.*, 2019, **119**, 8131–8191.

45 J. Bloino, A. Baiardi and M. Biczysko, *Int. J. Quantum Chem.*, 2016, **116**, 1543–1574.

46 V. Barone, *WIREs Comput. Mol. Sci.*, 2016, **6**, 86–110.

47 V. Barone, A. Baiardi, M. Biczysko, J. Bloino, C. Cappelli and F. Lipparini, *Phys. Chem. Chem. Phys.*, 2012, **14**, 12404–12422.

48 F. Muniz-Miranda, A. Pedone, G. Battistelli, M. Montalti, J. Bloino and V. Barone, *J. Chem. Theory Comput.*, 2015, **11**, 5371–5384.

49 C. Latouche, D. Skouteris, F. Palazzetti and V. Barone, *J. Chem. Theory Comput.*, 2015, **11**, 3281–3289.

50 D. Jacquemin, E. Brémond, A. Planchat, I. Ciofini and C. Adamo, *J. Chem. Theory Comput.*, 2011, **7**, 1882–1892.

51 E. Stendardo, F. Avila Ferrer, F. Santoro and R. Improta, *J. Chem. Theory Comput.*, 2012, **8**, 4483–4493.

52 J. Liu and W. Liang, *J. Chem. Phy.*, 2011, **135**, 014113.

53 M. Fortino, E. Collini, A. Pedone and J. Bloino, *Phys. Chem. Chem. Phys.*, 2020, –.

54 É. Brémond, M. E. Alberto, N. Russo, G. Ricci, I. Ciofini and C. Adamo, *Phys. Chem. Chem. Phys.*, 2013, **15**, 10019–10027.

55 R. Improta, V. Barone and F. Santoro, *Angew. Chem. Int. Ed.*, 2007, **46**, 405–408.

56 A. Stoliaroff, J. Rio and C. Latouche, *New J. Chem.*, 2019, **43**, 11903–11911.

57 S. Di Tommaso, D. Bousquet, D. Moulin, F. Baltenneck, P. Riva, H. David, A. Fadli, J. Gomar, I. Ciofini and C. Adamo, *J. Comput. Chem.*, 2017, **38**, 998–1004.

58 D. Jacquemin, E. Brémond, I. Ciofini and C. Adamo, *J. Phys. Chem. Lett.*, 2012, **3**, 468–471.

59 J. C. Slater, *The Self-Consistent Field for Molecular and Solids, Quantum Theory of Molecular and Solids*, McGraw-Hill, New York, 1974, vol. 4.

60 S. H. Vosko, L. Wilk and M. Nusair, *Can. J. Phys.*, 1980, **58**, 1200–1211.

61 J. P. Perdew, K. Burke and M. Ernzerhof, *Phys. Rev. Lett.*, 1996, **77**, 3865–3868.

62 A. D. Becke, *J. Chem. Phys.*, 1993, **98**, 5648–5652.

63 V. Barone, L. Orlandini and C. Adamo, *Chem. Phys. Lett.*, 1994, **231**, 295–300.

64 P. J. Stephens, F. J. Devlin, M. J. Frisch and C. F. Chabalowski, *J. Phys. Chem.*, 1994, **98**, 11623–11627.

65 C. Adamo and V. Barone, *J. Chem. Phys.*, 1999, **110**, 6158–6170.

66 M. Ernzerhof and G. E. Scuseria, *J. Chem. Phys.*, 1999, **110**, 5029–5036.

67 Y. Zhao, N. E. Schultz and D. G. Truhlar, *Theor. Chem. Acc.*, 2008, **120**, 215–241.

68 A. D. Boese and J. M. L. Martin, *J. Chem. Phys.*, 2004, **121**, 3405–3416.

69 Y. Zhao and D. G. Truhlar, *J. Phys. Chem.*, 2006, **110**, 5121–5129.

70 Y. Zhao and D. G. Truhlar, *J. Phys. Chem. A*, 2006, **110**, 13126–13130.

71 T. Yanai, D. Tew and N. Handy, *Chem. Phys. Lett.*, 2004, **393**, 51–57.

72 J.-D. Chai and M. Head-Gordon, *Phys. Chem. Chem. Phys.*, 2008, **10**, 6615–6620.

73 M. J. Frisch, G. W. Trucks, H. B. Schlegel, G. E. Scuseria, M. A. Robb, J. R. Cheeseman, G. Scalmani, V. Barone, G. A. Petersson, H. Nakatsuji, X. Li, M. Caricato, A. V. Marenich, J. Bloino, B. G. Janesko, R. Gomperts, B. Mennucci, H. P. Hratchian, J. V. Ortiz, A. F. Izmaylov, J. L. Sonnenberg, D. Williams-Young, F. Ding, F. Lipparini, F. Egidi, J. Goings, B. Peng, A. Petrone, T. Henderson, D. Ranasinghe, V. G. Zakrzewski, J. Gao, N. Rega, G. Zheng, W. Liang, M. Hada, M. Ehara, K. Toyota, R. Fukuda, J. Hasegawa, M. Ishida, T. Nakajima, Y. Honda, O. Kitao, H. Nakai, T. Vreven, K. Throssell, J. A. Montgomery, Jr., J. E. Peralta, F. Ogliaro, M. J. Bearpark, J. J. Heyd, E. N. Brothers, K. N. Kudin, V. N. Staroverov, T. A. Keith, R. Kobayashi, J. Normand, K. Raghavachari, A. P. Rendell, J. C. Burant, S. S. Iyengar, J. Tomasi, M. Cossi, J. M. Millam, M. Klene, C. Adamo, R. Cammi, J. W. Ochterski, R. L. Martin, K. Morokuma, O. Farkas, J. B. Foresman and D. J. Fox, *Gaussian'16 Revision B.01*, 2016, Gaussian Inc. Wallingford CT.

74 T. Clark, J. Chandrasekhar, G. W. Spitznagel and P. V. R.

Schleyer, *J. Comput. Chem.*, 1983, **4**, 294–301.
75 P. C. Hariharan and J. A. Pople, *Theor. Chim. Acta*, 1973, **28**, 213–222.
76 W. J. Hehre, R. Ditchfield and J. A. Pople, *J. Chem. Phys.*, 1972, **56**, 2257–2261.
77 R. Ditchfield, W. J. Hehre and J. A. Pople, *J. Chem. Phys.*, 1971, **54**, 724–728.
78 J. Tomasi, B. Mennucci and R. Cammi, *Chem. Rev.*, 2005, **105**, 2999–3094.
79 E. Cancès, B. Mennucci and J. Tomasi, *J. Chem. Phys.*, 1997, **107**, 3032–3041.
80 F. Santoro, A. Lami, R. Improta, J. Bloino and V. Barone, *J. Chem. Phys.*, 2008, **128**, 224311.
81 F. Santoro, A. Lami, R. Improta and V. Barone, . *Chem. Phys.*, 2007, **126**, 184102.
82 É. Brémond, M. Savarese, C. Adamo and D. Jacquemin, *J. Chem. Theory Comput.*, 2018, **14**, 3715–3727.
83 É. Brémond, M. Savarese, N. Q. Su, Á. J. Pérez-Jiménez, X. Xu, J. C. Sancho-García and C. Adamo, *Journal of Chemical Theory and Computation*, 2016, **12**, 459–465.
84 J. P. Perdew, A. Ruzsinszky, L. A. Constantin, J. Sun and G. I. Csonka, *J. Chem. Theory Comput.*, 2009, **5**, 902–908.
85 A. J. Cohen, P. Mori-Sánchez and W. Yang, *Science*, 2008, **321**, 792–794.
86 A. Dreuw and M. Head-Gordon, *J. Am. Chem. Soc.*, 2004, **126**, 4007–4016.
87 E. Brémond, M. Savarese, A. J. Pérez-Jiménez, J. C. Sancho-García and C. Adamo, *J. Phys. Chem. Lett.*, 2015, **6**, 3540–3545.